

Can We Remove the Ground? Obstacle-aware Point Cloud Compression for Remote Object Detection

Pengxi Zeng¹, Alberto Presta^{2*}, Jonah Reinis³,
Dinesh Bharadia¹, Hang Qiu⁴, and Pamela Cosman¹

Abstract—Efficient point cloud (PC) compression is crucial for streaming applications, such as augmented reality and cooperative perception. Classic PC compression techniques encode all the points in a frame. Tailoring compression towards perception tasks at the receiver side, we ask the question, "Can we remove the ground points during transmission without sacrificing the detection performance?" Our study reveals a strong dependency on the ground from state-of-the-art (SOTA) 3D object detection models, especially on those points below and around the object. In this work, we propose a lightweight obstacle-aware Pillar-based Ground Removal (PGR) algorithm. PGR filters out ground points that do not provide context to object recognition, significantly improving compression ratio without sacrificing the receiver side perception performance. Not using heavy object detection or semantic segmentation models, PGR is light-weight, highly parallelizable, and effective. Our evaluations on KITTI and Waymo Open Dataset show that SOTA detection models work equally well with PGR removing 20-30% of the points, with a speeding of 86 FPS.

I. INTRODUCTION

Point cloud streaming enables various applications, such as augmented reality, sensor fusion, and cooperative perception [1], [2], [3]. For example, in the context of connected and automated vehicles (CAVs), merging data from peer vehicles enhances situation awareness beyond individual on-board sensing capabilities [5], [6], [7]. However, storing and transmitting point clouds from LiDAR (Light Detection and Ranging) sensors is costly. A point cloud (PC) frame is represented as an array of points, each with (x, y, z) spatial coordinates and associated attributes, such as reflectance. A 64-line LiDAR generates around 100,000 points per frame, meaning that at 10 FPS scanning rate, the raw data rate of 128 Mbps exceeds the available bandwidth of current vehicle-to-infrastructure (V2I) communication technologies, such as C-V2X [8]. Therefore, it is necessary to develop efficient systems for vehicular LiDAR data transmission.

The main challenges of designing such efficient systems end-to-end are twofold: 1) a data compression technique that can fit narrow communication bandwidth in which the compressed representation is suitable for remote machine vision tasks, and 2) a low-latency compression pipeline that supports latency-sensitive machine vision tasks. To reduce data volume, previous work [9] exploits the redundancy in the raw frame to compress the point cloud in a lossless

fashion [10], or slightly trades off the fidelity for a lower bit rate [11]. However, manipulated data in the compression process, though sometimes indistinguishable by human eyes, can significantly degrade machine vision performance. To preserve performance, machine vision models such as object detection and semantic segmentation can be used *before* quantization, but this approach only transmits incomplete or encoded information, limiting downstream tasks. In addition, these models often add significant latency, hindering real-time streaming applications. In this paper, we explore an efficient design that achieves low-latency compression without sacrificing application accuracy. Taking object detection as an example, the performance dependency on each point varies significantly. Fig. 1 shows the objects detected by PVT-SSD [47] using the original PC (left), and using the PC after removing ground points (middle) with a semantic segmentation model PolarNet [26]. It illustrates that naively removing ground points based only on semantics may negatively impact perception performance, as state-of-the-art (SOTA) models show strong dependency on certain ground points. Our key idea is to investigate the feasibility of wisely removing irrelevant context (*i.e.* partial ground in this case), while maintaining the performance of downstream computer vision tasks (Fig. 1 right).

Our main contributions are: (a) A feasibility and innovative study demonstrating that *a careful selection* of ground points can be removed with minimal impact on detection accuracy, (b) Experimental results on the value of retaining partial ground points close to objects, and (c) A lightweight, highly parallelizable Pillar-based Ground point Removal (PGR) algorithm that is able to selectively retain most ground points near objects without the complexity of detecting objects.

II. RELATED WORK

A. Point Cloud Compression

A PC $X = \{p_i \in \mathbb{R}^d\}_1^N$, is a set of N points in 3D space, where each point p_i consists of spatial coordinates x_i, y_i, z_i , and additional attributes such as RGB color and reflectance. Unlike images, this data is unstructured; the points are situated within a vast 3D space characterized by local density but sparse distribution overall. To efficiently compress a PC, it has to be first converted to a data structure that can represent position data compactly, allowing exploitation of inter-point attribute correlation. One approach uses a tree structure [10], [12], [13], [14], suitable for representing data with unevenly distributed point density. An octree-based PC compression algorithm was proposed in [10], compactly

¹Dept. of Electrical and Computer Engineering, UC San Diego, CA, USA

²Computer Science Department, University of Turin, Italy

³Case Western Reserve University, OH, USA

⁴ECE / CSE Dept., University of California Riverside, CA, USA

*Corresponding author, mail : alberto.presta@unito.it

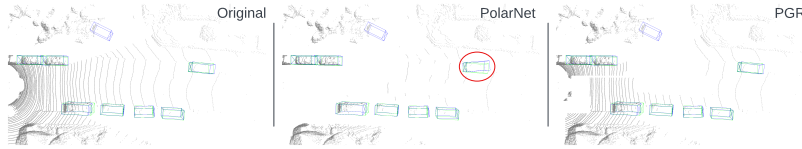


Fig. 1: Object ground truth (green) and detection results (blue) using PVT-SSD with an input of original (left) PC, PC with semantic ground removal (middle, PolarNet), and PC with PGR (right). Using PC with semantic ground removal, detection bounding boxes are mismatched with ground truth (red circle), while PGR does not affect detection performance.

describes occupancy in 3D space. Draco [15] uses KD-trees to depict PC geometry. Additionally, MPEG [14] has introduced a standard for encoding and decoding octree-based PCs, enabling compression based on geometry (G-PCC); we exploited this algorithm in our work.

B. Ground Point Removal

We categorize Lidar ground point removal methods into non-learning-based methods, which employ handcrafted techniques for ground segmentation, and learning-based methods, which use deep learning. In the former group, older methods such as [18] partitioned PCs to estimate ground points by comparisons with local line fits, while [19] exploited a graph-based approach to segment ground and objects based on local convexity measures. A two-step algorithm [20] identified the ground surface iteratively by using deterministically assigned seed points and clustering the remaining non-ground points, leveraging the structure of the Lidar PC, and [21] detected most non-ground points based on inter-ring distances, then used multi-region RANSAC plane fitting to separate the remaining non-ground. More recently, [22] used a recursive algorithm to obtain a 2D elevation map to estimate terrain and segment the PC, while [23] encoded a PC into a Concentric Zone Model-based representation, followed by ground plane fitting and ground likelihood estimation to extract the final ground segmentation.

Among learning-based methods, [24] estimated the ground plane elevation end-to-end with a grid-based representation, exploiting PointNet [25] to extract features and regressing ground height for each cell of the grid. In [26], a polar bird’s-eye-view representation balanced the points across grid cells in a polar coordinate system and aligned the attention of a segmentation network with the long-tailed distribution of points along the radial axis. For segmentation, they exploited a simplified KNN-free PointNet to transform points to a fixed-length representation, and then a ring CNN that outputs a quantized prediction, decoded finally to the point domain.

C. Object Detection on Point Clouds

Existing methods for LiDAR 3D object detection can be classified into voxel-based, point-based, and point-voxel based methods. In voxel-based methods [27], [28], [29], [30], [32], a PC is partitioned into regular spaces called voxels, and features extracted from voxels are fed into deep neural networks. VoxelNet [28] and SECOND [29] represent seminal works of this approach, while PointPillars [30] further reduces computational complexity by defining pillars that

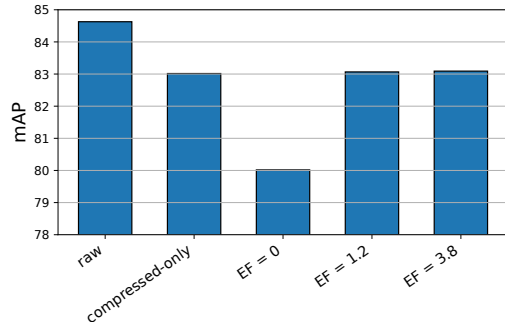


Fig. 2: Feasibility study on ground point removal for Car detection in KITTI Dataset. The evaluation ranges from uncompressed ‘raw’ PCs to ‘compressed-only’ without ground point removal, and then through a series of Extension Factors (EFs) combined with compression.

extend only along the vertical axis. Similarly, PillarNet [31] introduces a powerful encoder network for effective pillar feature learning and a neck network for spatial-semantic feature fusion. Point-based methods directly use the PC’s unstructured format without converting it into voxels. The pioneering work PointNet [25] was followed by extensive improvements [33], [34], [35], [36], [37]. Point-based methods use point sampling, which aims to select a representative subset of input points, and feature learning, which learns local features related to the selected points, to be used by subsequent object detection layers.

Since the transformer architecture [42], [43] has shown great ability in vision tasks, there have been works with transformers [44], [45], [46], [47]. PVT-SSD [47] uses a transformer architecture to associate contextual features from voxels and geometric features from points.

III. METHODS

A. Problem Statement

Given an input PC frame $X = \{p_i \in \mathbb{R}^d\}_1^N$, a ground point removal pre-processing algorithm f , a PC encoder g_{enc} , and a PC decoder g_{dec} , the encoded bitstream is $b = g_{enc}(f(X))$ while the decoded PC is represented as $Y = g_{dec}(b)$. Considering a downstream machine vision task T with its corresponding performance denoted $p_T(Y)$, the goal of this work is to find a suitable f that allows a significant bit rate reduction with a negligible sacrifice in terms of $p_T(Y)$. We focus only on the choice of f , and we maintain all other parts of the process fixed.

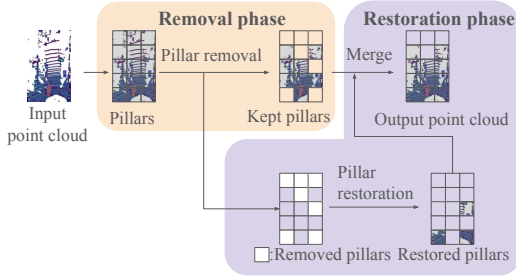


Fig. 3: Illustration of PGR with reduced number of pillars.

B. Impact of Ground Points on 3D Object Detection

In this part we examine how the total or partial removal of ground points impacts the performance of the downstream machine vision task. Starting from an input PC X , we consider a pre-processing algorithm $f(X) = \hat{X}$ that precisely removes selected ground points. We investigate the feasibility of this approach in an omniscient way, which means that we use the SOTA method PolarNet [26] to extract the ground points in a PC; the points labeled as ground in the segmentation result are used as a reference for ground point removal experiments.

In the experiments, we first removed all ground points and then restored those in the extended bounding boxes of objects annotated in ground-truth labels. The system can be described as:

$$\hat{X} = f(X; S, EF) \quad (1)$$

$$Y = g_{dec}(g_{enc}(\hat{X})) \quad (2)$$

where S is the per-point semantic segmentation result from PolarNet, and EF is an extension factor which controls how far we extend from the ground truth object bounding boxes. For example, if the ground truth bounding box for a car has the size $(length, width, height)$, then using EF , we restore any ground points extracted by PolarNet in the box of size $(1 + EF) \times (length, width, height)$. When $EF = 0$, it means that no extension is applied and only the annotated object points are restored. The PC after pre-processing will be compressed and decompressed with the standard geometry-based PC compression method G-PCC [14]. The decompressed point cloud Y is used for downstream task performance evaluation.

We exploit PVT-SSD [47] to study the performance degradation introduced by ground point removal. We compare omniscient point removal with a baseline where the raw PC is encoded without any point removed ($\hat{X} = X$). Using different extension factors, we found (Fig. 2) that for the Car class, removing all ground points degrades detection accuracy by more than 3%. However, with $EF \in [0.3, 3.6]$, the partial removal of ground points allows the system to achieve the same detection accuracy as for a compressed PC with no ground points removed, but at significantly lower bit rates. This indicates that *while full removal of the ground points outside of the object bounding boxes hurts detection, partial removal holds potential for rate savings without sacrificing detection.*

C. Pillar-based Ground Removal Algorithm

The observation from the feasibility study gives us intuition on designing a pillar-based ground removal (PGR) algorithm that removes ground points that are not near objects. As shown in Fig. 3, our method has two steps, **Pillar removal** and **Pillar restoration**.

1) *Pillar removal*: Starting from the assumption that in a sufficiently small region composed of only ground points, there would be little difference in height, every input frame is split into a 2D grid of square pillars pl_j for $j = \{1, \dots, M\}$, where M is the total numbers of pillars. The pillar size, or *resolution*, determines the granularity at which the overall algorithm operates. The goal is to remove pillars that are likely part of the ground. For each pillar, if the height difference between its highest and lowest points is below a certain threshold, then it might contain only ground points. For a pillar pl_i , this condition is written as:

$$d_z(pl_i) = z_{max}(pl_i) - z_{min}(pl_i) \leq \delta_{minmax} \quad (3)$$

where $z_{max}(pl_i)$ and $z_{min}(pl_i)$ are the maximum and minimum heights in the pillar, and δ_{minmax} is a threshold.

However, this condition is insufficient— if for example, a pillar passes through the roof of a car, it is possible that the height difference is small because this area is quite flat; erroneously detecting these points as ground would mistakenly remove a portion of the car. In addition to the condition on height difference, one needs to consider the neighboring area and a *local ground baseline*. We compare $z_{min}(pl_i)$ with the height b of the lowest point in a square neighborhood controlled by a parameter *environmental radius* (er), representing half of the side length. A pillar is considered to be ground if it fulfills condition (3) and also the following one:

$$d_{env}(pl_i) = z_{min}(pl_i) - b < \delta_{env}. \quad (4)$$

Summing up, the pillar removal step consists of an indicator function Φ_i :

$$\Phi_i = \begin{cases} 0 & \text{if } d_z(pl_i) \leq \delta_{minmax} \text{ and } d_{env}(pl_i) < \delta_{env} \\ 1 & \text{otherwise} \end{cases} \quad (5)$$

Parameter choices should generally be based on physical aspects of PCs rather than the nature of a specific dataset. Concerning δ_{minmax} , it should be large enough to allow sidewalk curbs (typically 10-20cm) as well as somewhat taller street medians to be considered ground points and removed, and yet small enough to avoid deleting small pedestrians (typical 2-year-old children are 80-95cm tall); So we set δ_{minmax} to 40cm. We set er to 1.8m, roughly the width of a standard car, aiming to ensure that a pillar containing only a flat car roof will get compared with the local ground baseline and not be declared as ground points. We set δ_{env} to 40cm, to ensure that a flat car roof or even the top of a flat baby stroller is differentiated from the local ground baseline. We emphasize that these values are based on physical characteristics of the environment

rather than on individual datasets, which should enhance the algorithm’s robustness. Lastly, a smaller *resolution* means that we consider smaller pillars. The choice trades off grid granularity and model speed; empirically we set it to 40cm.

2) *Pillar restoration*: The *Pillar removal* stage can remove points close to an object; however, we observed in Sec. III-B that we need ground points in the vicinity of objects for better detection precision. Operating on the pillar level, the *Pillar restoration* step restores some previously removed pillars. If a removed pillar pl_i is close enough to at least one retained pillar, then preserving pl_i is likely to be useful for the machine vision task. A removed pillar pl_i is restored if there exists any pillar pl_j retained during the removal phase such that the Chessboard distance between their centers is below a threshold δ_{res} . We use R_i to denote a restoration flag indicating whether to restore pl_i :

$$R_i = \begin{cases} 1 & \text{if } \sum_{j|D(i,j) \leq \delta_{res}} \Phi_j > 0 \\ 0 & \text{otherwise.} \end{cases} \quad (6)$$

As points become sparser farther from the Lidar, objects may lose critical points that contain information about their global geometry. Such important points could be close to the ground and thus removed in the removal phase, but cannot be restored if δ_{res} is not large enough. To strike a good trade-off between removal efficiency and detection precision, we adapt δ_{res} for different ranges. From the experiments, for pillars closer than 30m, we used $\delta_{res,1} = 1.8\text{m}$ for KITTI and $\delta_{res,1} = 2.2\text{m}$ for the Waymo Open Dataset. For both datasets, we used $\delta_{res,2} = 5.4\text{m}$ for pillars further away. Due to the sparsity of points in far ranges, a large δ_{res} will cause only a slight increase in the number of ground points remaining.

Fig. 3 depicts the preprocessing framework, which is not recursive and is applied only once, obtaining real-time runtime.

IV. EXPERIMENTS

A. Experimental Setup

We selected six configurations of geometry scaling factors (0.01, 0.012, 0.015, 0.022, 0.035, 0.063) paired up with six attribute quantization parameters (34, 30, 26, 22, 18, 14). The bit rate of the compressed PC is represented by bits per point (bpp), obtained by dividing the total number of bits in the compressed frame representation by the total number of points in the PC for that frame.

We use object detection to evaluate the effectiveness of PGR. The PC after applying PGR is compressed and decompressed and subsequently sent through pre-trained object detection models. We used **Mean Average Precision (mAP)** as the detection performance metric for each class [52].

B. Datasets

1) *KITTI*: The KITTI dataset [49] contains 7481 training samples and 7518 test samples. The training samples are commonly divided into a training set with 3712 samples and a validation set with 3769 samples. Annotations are

provided for objects in the camera’s field of view. Objects are labeled into classes including Car, Pedestrian, and Cyclist. Depending on three factors (minimum bounding box size, occlusion level, and maximum truncation), the annotated objects are classified into easy, moderate, and hard difficulty levels. Common practice is to report performance metrics on moderate difficulty.

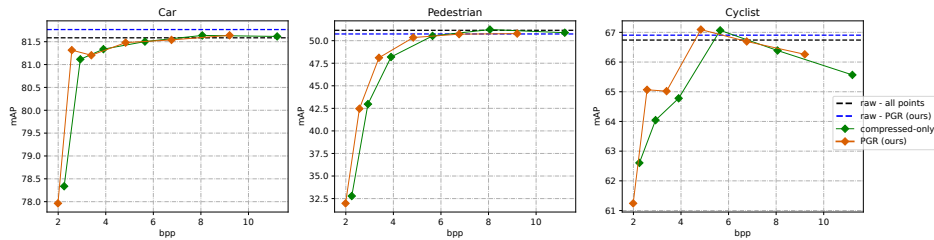
2) *Waymo*: The Waymo Open Dataset (WOD) [50] contains 798 scenes for training and 202 scenes for validation. Annotations are provided separately for Lidar and camera data. Based on the number of points contained, objects are classified into two difficulty levels, LEVEL_1 for those having more than five points, and LEVEL_2 for those having at least one point. Each Lidar data entry consists of the point’s (x, y, z) coordinates and attributes (intensity and elongation). Each frame may contain a *no-label zone* in which there are no ground truth annotations attempted, usually because the points are far from the sensor and difficult to annotate or considered unimportant. In this paper, we remove the points in the no-label zone since, without ground truth labels, these regions would not contribute meaningfully to the detection performance. WOD frames are in the format of a range image where pixel values represent the distance between the point and LiDAR, and two attributes, intensity and elongation, are given. In the experiments, we transformed the range image format to 3D format where each entry contains a point’s coordinates and attributes in 32-bit float.

C. PGR Performance on Object Detection

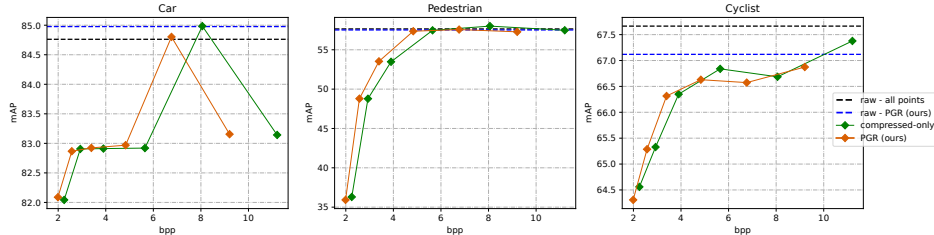
In this section, we evaluate the effectiveness of PGR as a preprocessing function before encoding the PC, considering two different object detection models, SECOND [29] and PVT-SSD [47].

1) *bpp vs. mAP*: Figures 4 and 5 show the bpp vs. MaP for the two datasets. Solid lines depict results with data compressed at various levels, with orange for PGR and green for the entire PC (no ground points removed). Dashed lines represent results on the raw dataset (no compression). Although the rate reduction depends on the operating point, PGR effectively shifts the rate-performance curve to the left, generally reducing the bitrate; this means we can achieve the same desired task performance with fewer bits. In Fig. 4, the PGR curve is above the non-processed curve for most of the range, for both models and all objects classes. For Waymo, there are gains for the Pedestrian and Cyclist classes, while for the Vehicle class, our curve is slightly below the compressed-only baseline. However, at lower bpp we can still observe an improvement, suggesting it may be of value to apply PGR in the low bit rate regime. The fraction of points that PGR removes depends on the frame, ranging from about 10% in dense urban areas to more than 50% in open ground.

Tab. I shows the average percentage of points that PGR preserves; it manages to remove a large portion of ground points with very little removal of relevant objects; in Fig. 5, comparing the lowest bit rate configurations, PGR achieves a 9.34% bit rate savings (0.282 bpp) with minimal mAP



(a) bpp vs mAP using SECOND.



(b) bpp vs mAP using PVT-SSD.

Fig. 4: bpp vs mAP on KITTI dataset using (a) SECOND and (b) PVT-SSD. Dotted lines represent results on uncompressed data. The up arrow \uparrow after mAP means that higher is better and the down arrow \downarrow after bpp means that lower is better.

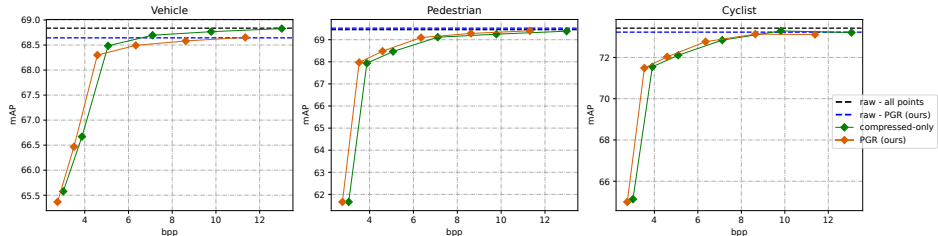


Fig. 5: bpp vs mAP on Waymo Open Dataset using PVT-SSD. Dotted lines represent results on uncompressed data.

changes: -0.209% (Vehicle), -0.003% (Pedestrian), and -0.154% (Cyclist) with respect to no GP removal. For the highest bit rate configurations, bit rate reduces by 12.94% (1.685 bpp) with mAP changes of -0.175%, +0.011%, and -0.078% for the respective classes.

2) *Run-time*: Algorithm complexity is important if ground point pre-processing were to be done in real time. On a GeForce RTX 3090 with 8 CPU cores, the speed to process frames sequentially (one by one), can reach 86.5 frames per second (fps), 11.6 ms per frame. This leaves ample latency budget for downstream tasks such as object detection, prediction, and segmentation.

TABLE I: Avg Percentage (%) of points preserved by PGR

Points Category	KITTI	Waymo
Car (KITTI) / Vehicle (WOD)	99.981	99.980
Pedestrian	99.995	99.982
Cyclist	99.995	99.988
Preserved points	75.133	82.415

D. Robustness with respect to parameter tuning

Robustness to parameter tuning is crucial for this type of system. Here, we evaluate the performance when varying

TABLE II: BD-mAP of our PGR with and without restoration phase, against SOTA method for point ground removal used as pre-processing and PVT-SSD as pre-trained model. We consider the case *compressed-only* as anchor.

	Car	Pedestrian	Cyclist
	BD-mAP	BD-mAP	BD-mAP
PGR (ours)	-0.14	1.75	0.008
PGR (ours) w/o restoration	-1.89	4.36	-0.57
GnDNet	-4.16	-13.72	-6.388
PolarNet	-1.42	-0.427	-0.95
patchwork++	-1.38	-0.97	-0.949

the parameters introduced in Sect. III. The parameters have specific real-world physical meanings that remain consistent across datasets (KITTI and Waymo) and object detection models. Fig. 6 shows the results of mAP vs. bpp on the KITTI dataset using SECOND, considering different configurations of our method. The orange line (PGR-c0) represents the standard configuration introduced in Sect. III, while in the other scenarios we manually changed parameters as follows:

- PGR-c1: er passes from 1.8 to 1.4.
- PGR-c2: $\delta_{res,1}$ passes from 1.8 to 1.4.
- PGR-c3: $\delta_{minmax} = 0.6$.
- PGR-c4: $(er, \delta_{minmax}, \delta_{res,1}, \delta_{res,2}) = (0.6, 0.35, 1.6, 5.2)$

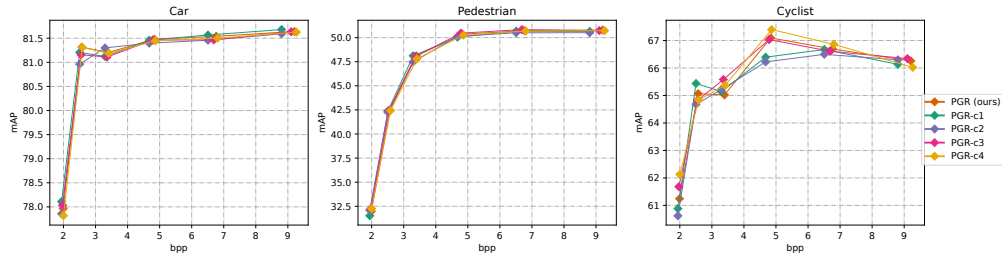


Fig. 6: bpp vs mAP on KITTI Dataset using SECOND, considering PGR with different configuration

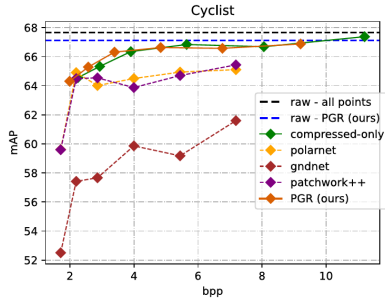


Fig. 7: bpp vs mAP of PGR against other ground point removal method considering Cyclist class.

Here we mention only the values that have been changed. The mAP remains similar in all configurations; for both *car* and *pedestrian* the differences are negligible, with only modest variations for the cyclist in the central bit range, without catastrophic degradation. Even for PGR-c4, where we modified 4 parameters, the final performance does not change remarkably, demonstrating the robustness of PGR to parameter tuning. Notably, the configurations for KITTI and Waymo in Sec. III are essentially the same, showing consistent performance in all datasets without significant parameter adjustments.

E. Comparison with other Ground Point Removal Methods

In this section, we compare PGR with other ground removal method used for pre-processing, namely PolarNet [26], GndNet [24], (deep-based methods) and patchwork++ [23] (handcrafted method). Table II shows results for KITTI using PVT-SSD as the pretrained model for object detection. We exploited Bjontegaard [4] metric considering mAP, recalling that a larger BD-mAP indicates better encoding efficiency. Although in the object detection scenario BD-mAP is not commonly used, they are well suited to summarize results across different compression levels.

PGR outperforms all models across all object classes, matching or exceeding the performance of the compressed-only anchor, where no ground points are removed. Fig. 7 further illustrates these results for the Cyclist class.

These results are consistent with Sec. III-B, where we show that removing all ground points leads to a marked performance degradation. While other methods aim to completely remove ground points, PGR preserves object detection performance with a careful selection of what part of the

ground could be removed harmlessly. Because of this, even if PGR may perform poorly in ground detection compared to other methods (75% of ground points are preserved in KITTI), we obtained the best results in terms of object detection. The goal of this work is to remove only that portion of the ground that does not degrade performance.

F. Ablation Study

Table II shows results with and without the PGR restoration phase. This phase aims to restore some points that were mistakenly removed in the algorithm’s first step. Despite an obvious slight gain in terms of bits saved, we observe a significant decrease in precision, especially for the Car and Cyclist classes. Without the restoration phase, we retain 98.076% of car points, 98.584% of cyclist points, and 98.844% of pedestrian points, values closely matching those in Tab. I with restoration; the latter class is the only one that presents some degradation after the restoration phase. This suggests that for smaller objects, detection models may require fewer ground points around them to provide context, and that with a more compact geometry, critical points are less likely to be lost during the removal phase.

V. CONCLUSION AND FUTURE WORKS

This work provides insight that some ground points are needed in PCs to enable remote detection of cars, pedestrians and cyclists. We then present a novel method to remove superfluous ground points. Following the intuition shown in Section III-B that portions of the ground close to objects could be useful for downstream machine vision tasks, we devised a two-step algorithm for targeted ground removal. First, we remove points that are most likely part of the ground, and then restore those points that are close enough to objects. Although simple, PGR produced excellent results in bit rate reduction, without compromising the final precision results for object detection, especially in low bit rate regimes, emphasizing also that PGR can be considered real-time, achieving a speed of 86.5 fps. We also showed in Sec. IV-E that our method is more suitable than other SOTA methods for this preprocessing, yielding better results for all objects considered, analyzing also in Sec. IV-F the impact of the restoration phase.

Future developments will focus on enhancing the algorithm’s robustness to uneven surfaces and small objects, and optimizing parameter selection using Bayesian optimization or evolutionary algorithms.

REFERENCES

- [1] Qiu, Hang, et al. "AutoCast: scalable infrastructure-less cooperative perception for distributed collaborative driving." *ACM MobiSys*. 2022.
- [2] Qiu, Hang, et al. "AVR: Augmented vehicular reality." In *International Conference on Mobile Systems, Applications, and Services*. 2018.
- [3] Chen, Q. et al. "F-cooper: Feature based cooperative perception for autonomous vehicle edge computing system using 3D point clouds". In *IEEE Symposium on Edge Computing*. 2019
- [4] Bjontegaard, Gisle. Calculation of average PSNR differences between RD-curves. In *VCEG-M33*, 2001
- [5] Wang, Tsun-Hsuan, et al. "V2VNet: Vehicle-to-vehicle communication for joint perception and prediction." In *European conference on computer vision*. 2020.
- [6] Xu, Runsheng, et al. "CoBEVT: Cooperative Bird's Eye View Semantic Segmentation with Sparse Transformers." In *Conference on Robot Learning*. PMLR, 2023.
- [7] Xu, Runsheng, et al. "V2X-ViT: Vehicle-to-everything cooperative perception with vision transformer." In *ECCV*, 2022.
- [8] Cui, Jiaxun, et al. "Coopernaut: End-to-end driving with cooperative perception for networked vehicles." In *Proceedings of the IEEE/CVF Conference on Computer Vision and Pattern Recognition*. 2022.
- [9] Graziosi, Danillo, et al. "An overview of ongoing point cloud compression standardization activities: Video-based (V-PCC) and geometry-based (G-PCC)." In *APSIPA Transactions on Signal and Information Processing*. 2020
- [10] Schnabel, Ruwen, and Reinhard Klein. "Octree-based Point-Cloud Compression." *PBG@ SIGGRAPH 3* (2006).
- [11] Schwarz, Sebastian, et al. "Emerging MPEG Standards for Point Cloud Compression." In *IEEE Journal on Emerging and Selected Topics in Circuits and Systems*, 2019
- [12] Elseberg, Jan et al. "One billion points in the cloud—an octree for efficient processing of 3D laser scans." In *Journal of Photogrammetry and Remote Sensing*, 2013
- [13] Schwarz, Sebastian, et al. "Emerging MPEG standards for point cloud compression." In *IEEE Journal on Emerging and Selected Topics in Circuits and Systems* ,2018, pp. 133-148.
- [14] *G-PCC codec description v12*, Output Document N 0151, ISO/IEC JTC 1/SC 29/WG 7, 2021
- [15] Huang, Tianxin, and Yong Liu. "3D point cloud geometry compression on deep learning." In *Proceedings of the 27th ACM international conference on multimedia*. 2019.
- [16] Goyal, Vivek K. "Theoretical foundations of transform coding." In *IEEE Signal Processing Magazine* 18.5 (2001): 9-21.
- [17] De Queiroz, Ricardo L., and Philip A. Chou. "Compression of 3D point clouds using a region-adaptive hierarchical transform." In *IEEE Transactions on Image Processing*, 2016
- [18] Himmelsbach, Michael, Felix V. Hundelshausen, and H-J. Wuensche. "Fast segmentation of 3D point clouds for ground vehicles." In *IEEE Intelligent Vehicles Symposium*, 2010.
- [19] Moosmann, Frank, Oliver Pink, and Christoph Stiller. "Segmentation of 3D lidar data in non-flat urban environments using a local convexity criterion." In *IEEE Intelligent Vehicles Symposium*, 2009.
- [20] Zermas, Dimitris, Izzat Izzat, and Nikolaos Papanikolopoulos. "Fast segmentation of 3D point clouds: A paradigm on lidar data for autonomous vehicle applications." In *IEEE International Conference on Robotics and Automation (ICRA)*, 2017.
- [21] Narksri, Patiphon, et al. "A slope-robust cascaded ground segmentation in 3D point cloud for autonomous vehicles." In *21st International Conference on intelligent transportation systems (ITSC)*, 2018.
- [22] Steinke, Nicolai et al. "GroundGrid:Lidar point cloud ground segmentation and terrain estimation." In *Robotics and Automation Letters*, 2023
- [23] Lim, Hyungtae et al. "Patchwork: Concentric zone-based region-wise ground segmentation with ground likelihood estimation using a 3D LiDAR sensor." In *IEEE Robotics and Automation Letters*, 2021
- [24] Paigwar, Anshul, et al. "GndNet: Fast ground plane estimation and point cloud segmentation for autonomous vehicles." In *International Conference on Intelligent Robots and Systems (IROS)*, 2020.
- [25] Qi, Charles R., et al. "PointNet: Deep learning on point sets for 3D classification and segmentation." In *Proceedings of the IEEE conference on computer vision and pattern recognition*, 2017.
- [26] Zhang, Yang, et al. "PolarNet: An improved grid representation for online lidar point clouds semantic segmentation." In *CVPR*, 2020.
- [27] Yang, Bin, Wenjie Luo, and Raquel Urtasun. "PIXOR: Real-time 3D object detection from point clouds." In *Proceedings of the IEEE conference on Computer Vision and Pattern Recognition*. 2018.
- [28] Zhou, Yin, and Oncel Tuzel. "VoxelNet: End-to-end learning for point cloud based 3D object detection." In *Proceedings of the IEEE conference on computer vision and pattern recognition*, 2018.
- [29] Yan, Yan, Yuxing Mao, and Bo Li. "SECOND: Sparsely embedded convolutional detection." In *Sensors*, 2018.
- [30] Lang, Alex H., et al. "PointPillars: Fast encoders for object detection from point clouds." In *Proceedings of the IEEE/CVF conference on computer vision and pattern recognition*, 2019.
- [31] Shi, Guangsheng, Ruifeng Li, and Chao Ma. "PillarNet: Real-time and high-performance pillar-based 3D object detection." In *European Conference on Computer Vision*, 2022
- [32] Wang, Yue, et al. "Pillar-based object detection for autonomous driving." In *European conference on computer vision*, 2020.
- [33] Qi, Charles Ruizhongtai, et al. "PointNet++: Deep hierarchical feature learning on point sets in a metric space." In *Advances in neural information processing systems*, 2017.
- [34] Shi, Shaoshuai, Xiaogang Wang, and Hongsheng Li. "PointRCNN: 3D object proposal generation and detection from point cloud." In *conference on computer vision and pattern recognition*, 2019.
- [35] Yang, Zetong, et al. "3DSSD: Point-based 3D single stage object detector." In *Proceedings of the IEEE/CVF conference on computer vision and pattern recognition*, 2020.
- [36] Pan, Xuran, et al. "3D object detection with pointformer." In *IEEE/CVF Conference on Computer Vision and Pattern Recognition*, 2021.
- [37] Shi, Weijing, and Raj Rajkumar. "Point-GNN: Graph neural network for 3D object detection in a point cloud." In *IEEE/CVF conference on computer vision and pattern recognition*, 2020.
- [38] Miao, Zhenwei, et al. "PVGNet: A bottom-up one-stage 3D object detector with integrated multi-level features." In *IEEE Conference on Computer Vision and Pattern Recognition*, 2021.
- [39] Shi, Shaoshuai, et al. "PV-RCNN: Point-voxel feature set abstraction for 3D object detection." In *Proceedings of the IEEE/CVF conference on computer vision and pattern recognition*, 2020.
- [40] Yang, Honghui, et al. "Graph R-CNN: Towards accurate 3D object detection with semantic-decorated local graph." In *ECCV*, 2022.
- [41] Ye, Maosheng et al. "HVNet: Hybrid voxel network for lidar based 3D object detection." In *Proceedings of the IEEE/CVF conference on computer vision and pattern recognition*, 2020.
- [42] Vaswani, Ashish, et al. "Attention is all you need." In *Advances in neural information processing systems*, 2017.
- [43] Dosovitskiy, Alexey, et al. "An Image is Worth 16x16 Words: Transformers for Image Recognition at Scale." In *International Conference on Learning Representations*. 2020.
- [44] Liu, Ze, et al. "Group-free 3D object detection via transformers." In *IEEE International Conference on Computer Vision*, 2021.
- [45] Misra, Ishan, Rohit Girdhar, and Armand Joulin. "An end-to-end transformer model for 3D object detection." In *Proceedings of the IEEE/CVF International Conference on Computer Vision*, 2021.
- [46] Wang, Haiyang, et al. "DSVT: Dynamic sparse voxel transformer with rotated sets." In *Proceedings of the IEEE/CVF Conference on Computer Vision and Pattern Recognition*, 2023.
- [47] Yang, Honghui, et al. "PVT-SSD: Single-Stage 3D Object Detector with Point-Voxel Transformer." In *Proceedings of the IEEE/CVF Conference on Computer Vision and Pattern Recognition*, 2023.
- [48] Fischler, Martin et al. "Random sample consensus: a paradigm for model fitting with applications to image analysis and automated cartography." In *Communications of the ACM* 24.6, 1981
- [49] Geiger, Andreas, et al. "Are we ready for autonomous driving? the kitti vision benchmark suite." In *IJCP*, 2012.
- [50] Sun, Pei, et al. "Scalability in perception for autonomous driving: Waymo open dataset." In *Proceedings of the IEEE/CVF conference on computer vision and pattern recognition*, 2020.
- [51] *Common Test Conditions for G-PCC*, Output Document N 19584, ISO/IEC JTC 1/SC 29/WG 11, 2020
- [52] Everingham et al. "The pascal visual object classes challenge: A retrospective." In *IJCP*, 2015
- [53] Everingham, Mark, et al. "The pascal visual object classes (voc) challenge." In *International journal of computer vision*, 2010